Engineering Applications of Computational Fluid Mechanics Vol. 5, No. 2, pp. 247–258 (2011)

NUMERICAL INVESTIGATION OF FLOW PATTERNS IN RECTANGULAR SHALLOW RESERVOIRS

Matthieu Dufresne*, Benjamin J. Dewals†, Sébastien Erpicum, Pierre Archambeau and Michel Pirotton

University of Liège (ULg), ArGEnCO Department, MS²F Sector, Hydrology, Applied Hydrodynamics and Hydraulic Constructions (HACH), Chemin des chevreuils, 1, bât B52/3, étage +1, 4000 Liège, Belgium
** E-Mail: matthieu.dufresne@free.fr* (*Corresponding Author*)
† Belgian fund for scientific research (F.R.S.-FNRS)

ABSTRACT: In this study, the capability of a two-dimensional shallow-water numerical model to simulate the symmetric and asymmetric flows that can take place in rectangular shallow reservoirs with different lateral expansion ratios and dimensionless lengths is investigated. Numerically, the main difficulty is to properly reproduce the transition between symmetric and asymmetric flows. For a large lateral expansion ratio, the use of two protocols of simulation highlighted a high sensitivity of the simulated flow pattern to the initial condition. Comparison between simulated results and experimental data showed a good agreement for the critical shape parameter (combination of the lateral expansion ratio and the dimensionless length) between symmetric and asymmetric flows. A good agreement was also found for the value of the shorter reattachment length of asymmetric flows. For small lateral expansion ratios, the agreement was not so good. The model was used for even larger lateral expansion ratios in order to numerically extend the experimental dataset. This predictive work showed that the shape parameter, whose expression was only based on experiments carried out for small lateral expansion ratios, was also relevant for larger values. Moreover, the predicted values of the shorter reattachment length were also consistent with a regression only based on experimental results.

Keywords: rectangular shallow reservoirs, flow patterns, symmetry, asymmetry, reattachment

1. INTRODUCTION

Flow detachment and reattachment processes are common occurrences in hydraulic engineering; examples are flows over lateral expansions (Abbott and Kline, 1962; Chu et al., 2004), flows in groyne fields (Uijttewaal et al., 2001; Yeo et al., 2005), flows in tanks (Stovin and Saul 1994; Oca et al., 2004), etc., more generally all flows in structures with sudden geometrical variations. The present study focuses on turbulent free-surface flow in rectangular shallow reservoirs in the context of reservoir sedimentation. Sediment transport will be taken into account in the future since it is the long-term objective of the present study; practical applications are stormwater storage tanks (Kowalski et al., 1999; Todeschini et al., 2010), irrigation basins (Garde et al. 1990; Ranga Raju et al, 1999), reservoirs (Jothiprakash and Garg, 2008), side weir overflows (Luyckx et al., 1999), etc. As illustrated in Fig. 1, the geometry consists of an upstream expansion and a downstream contraction, which may lead – despite the symmetry – to an asymmetric flow pattern (Kantoush et al., 2008a).

If it is assumed that the flow is governed by the length of the reservoir (L), the lateral expansion (ΔB), the width of the inlet and outlet channels (b), the water depth (h), the mean depth-averaged velocity (U), the bed shear stress (τ), the water density (ρ), the water viscosity (μ) and the gravitational acceleration (g) – which are a set of nine variables involving time, mass and length units – dimensional analysis principles can reduce the problem to six dimensionless parameters (Langhaar, 1951). For example, one can choose a lateral expansion ratio ($\Delta B/b$), a dimensionless length ($L/\Delta B$), a dimensionless water depth ($h/\Delta B$), a Froude number ($U/(gh)^{0.5}$), a Reynolds number ($4\rho Uh/\mu$), and a bed friction number ($c_f \Delta B/2h$). Here, c_f is the bed friction coefficient ($2\tau/\rho U^2$); it can be estimated using a 'Colebrook' formula (see for example Henderson, 1966, p. 95).

Abbott and Kline (1962) intensively studied the stall of turbulent free surface flows over double lateral expansions (without downstream contraction). They showed that the recirculation zones in each side of the expansion were equal in length for lateral expansion ratios lower than 0.25 (flow pattern S2 in Fig. 2), and different for

Received: 23 Aug. 2010; Revised: 2 Jan. 2011; Accepted: 7 Jan. 2011

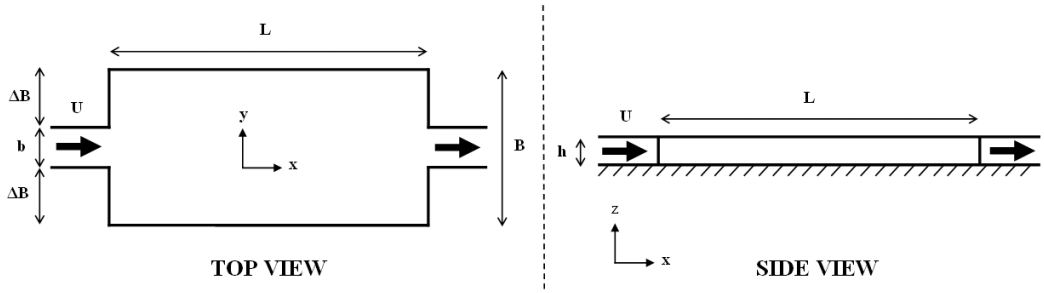

Fig. 1 Schemes of a rectangular shallow reservoir.

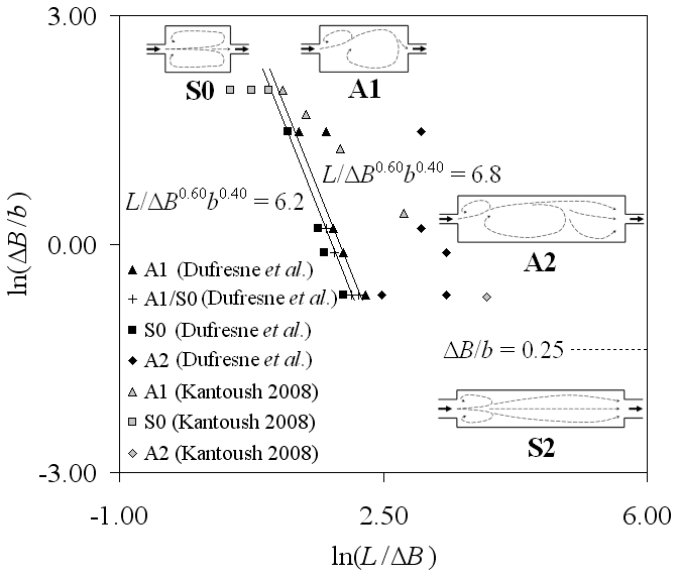

Fig. 2 Classification diagram of flow patterns in rectangular shallow reservoirs (valid for high water depths, high Reynolds numbers, low bed friction numbers and a Froude number of 0.20). The two lines correspond to the shape parameter of Dufresne et al. (2010): for values below 6.2, the flow is symmetric and for values higher than 6.8 the flow becomes asymmetric.

lateral expansion ratios greater than 0.25 (flow pattern A2). Kantoush (2008) showed that decreasing the dimensionless length of a shallow water reservoir induced a transition from an asymmetric flow to a symmetric flow without any reattachment (flow pattern S0). A reattachment point is defined as a point where the longitudinal velocity is zero and is changing its sign. Using the data of Kantoush (2008) and our own experimental results obtained for four different lateral expansion ratios (Dufresne et al., 2010) at high water depths (> 0.200 m above which the water depth has no influence on the flow pattern), high Reynolds numbers (around 220,000), low bed friction numbers (around 0.002–0.003) and a Froude number of 0.20, a transition criterion was identified as a combination of the dimensionless length and the lateral expansion ratio rather than only the dimensionless length (Dufresne et al., 2010):

Shape parameter

$$= \left(\frac{L}{\Delta B}\right)\left(\frac{\Delta B}{b}\right)^{0.40} = \frac{L}{\Delta B^{0.60} b^{0.40}} \quad (1)$$

When the criterion, named "shape parameter", was lower than approximately 6.2, the flow was symmetric (S0); it was asymmetric when the shape parameter was greater than approximately 6.8 (one or two reattachment points – flow patterns A1 or A2 – depending on the length of the reservoir); between these two values, the flow consisted of non-periodic fluctuations between symmetric and asymmetric patterns (A1/S0). Fig. 2 is a classification diagram. Since the flow was turbulent, it has to be noted that the experimental reattachment lengths (longitudinal distance between the upstream face of the reservoir and the reattachment point) given in the present paper are median values; the reattachment lengths fluctuated over a small distance on the reservoir wall. For example, the median value and the standard deviation of the reattachment length were respectively 1.18 m and 0.10 m for Experiment F4-a (ΔB = 0.35 m; $\Delta B/b$ = 1.23; $L/\Delta B$ = 20.0; $h/\Delta B$ = 0.57; $4\rho Uh/\mu$ = 210,000; $U/(gh)^{0.5}$ = 0.20; $c_f \Delta B/2h$ = 0.003; see Dufresne et al., 2010 for details).

For the flow pattern A2 ("long" reservoirs), increase of the Froude number induces a decrease

of the shorter reattachment length (R1); increase of the dimensionless water depth has the same effect until the shorter reattachment length reaches a minimum level (Dufresne et al., 2010). For the flow pattern A1 near the transition A1 – S0 ("short" reservoirs), when decreasing the water depth (but increasing the Froude number in the same time), Kantoush (2008) showed that the flow was not steady anymore but started to meander. For these fully turbulent flows, the influence of the Reynolds number is generally not significant (Abbott and Kline, 1962) but sometimes not completely negligible for the shorter reattachment length (Casarsa and Giannattasio, 2008). A significant influence of the bed friction number is only encountered for high values of this parameter (around 0.05–0.10), namely when the water depth is very low and/or the roughness is important (Chu et al., 2004; Babarutsi and Chu, 1991; Babarutsi et al., 1989).

Numerically, the main difficulty is to properly reproduce the transition between symmetric and asymmetric flows. Numerical studies mainly focused on the laminar case for which the flow symmetry could be broken by increasing the Reynolds number (see for examples Revuelta, 2005 and Battaglia and Papadopoulos, 2006 for sudden expansions, Mizushima and Shiotani, 2001 for expanded and contracted part); only a few numerical studies were carried out for the turbulent case (De Zilwa et al., 2000; Mullin et al., 2003). Even if the present study focused on fully turbulent flows, a number of studies undertaken at low and moderate Reynolds numbers give useful information in the context of symmetry breaking: Mullin et al. (2003) about the influence of geometrical imperfections, Wahba (2007) about the influence of the inflow velocity profile, Takaoka et al. (2009) about the propagation of a disturbance added at the inlet of the domain. Concerning turbulent free-surface flows in rectangular shallow reservoirs, Dewals et al. (2008) simulated symmetric and asymmetric flows by introducing a disturbance in the inlet discharge profile; another strategy consists of using an asymmetric initial velocity condition (Dufresne, 2008). Numerical simulations of flow in rectangular shallow reservoirs were also carried out by Kantoush et al. (2008b) but the authors omitted the presentation of their strategy to reproduce flow asymmetry.

The aim of the present study was to investigate the capability of a two-dimensional numerical model to simulate the symmetric and asymmetric flows that can be encountered in rectangular shallow reservoirs varying the lateral expansion ratio and the dimensionless length (see Dufresne et al., 2010 for a complete description of the experimental programme). After validation, the model was used as a prediction tool to extend the experimental results and get additional knowledge about the influence of the geometry on the flow pattern.

2. NUMERICAL MODEL

Numerical simulations were performed with the finite volume code Wolf 2D, developed at the University of Liège (Dewals, 2006; Erpicum, 2006, Erpicum et al., 2009 & 2010). The model is based on the two-dimensional depth-averaged equations of volume and momentum conservation, namely the "shallow-water" equations (see for example Dewals et al., 2008 for the set of equations); the choice of this approach is justified by the "reasonable" two-dimensionality of the flow that was confirmed by dye visualization during experiments (Dufresne et al., 2010). Three-dimensional turbulence processes are partly accounted for through the two-length scale k-ε turbulence closure, as detailed below.

Complementarily, in experimental work of Kantoush (2008) with a similar geometric setup, measured vertical velocity components using ultrasonic velocity profiler were verified to remain low compared to velocity components in the horizontal plane (Kantoush et al., 2008a) and two-dimensional numerical models were applied (Kantoush et al., 2008b), yet without careful consideration for the inflow boundary conditions as done here and in our previous work (Dewals et al., 2008).

In the shallow-water approach, the friction makes the link between the bed shear stress and the depth-averaged velocity. In the present study, the friction coefficient was modeled with the Colebrook formula (Idel'cik, 1969):

$$\frac{1}{\sqrt{4c_f}} = -2\log_{10}\left(\frac{k_S}{14.8h} + \frac{2.51}{\mathrm{Re}\sqrt{4c_f}}\right) \qquad (2)$$

Here, k_s is the equivalent grain roughness (zero in the present study since the walls are made of glass) and Re is the Reynolds number.

In the set of equations, bottom and vertical wall friction were taken into account in the friction source terms through a formulation developed by the second author (Dewals, 2006) and used by Dewals et al. (2008), Erpicum et al. (2009 & 2010) and Roger et al. (2009) among others.

The effect of turbulence on the mean flow was modeled using the Boussinesq approximation. The eddy viscosity was computed by a depth-averaged k-ε model with two different length scales accounting for vertical and horizontal turbulent mixing. This turbulence model is based on the work of Barbarutsi and Chu (1998) and was further developed by Erpicum (2006) and Erpicum et al. (2009). The use of the Colebrook friction model and the *k-ε* turbulence model freed us of any calibration procedure.

Table 1 summarizes the flow conditions with the dimensionless parameters given in the introduction. In this table, U is the cross-sectional averaged velocity in the inlet channel. As in the experiments (Dufresne et al., 2010), four lateral expansion ratios were investigated with numerical modeling: 0.52 (corresponding to $\Delta B = 0.25$ m and $b = 0.48$ m), 0.89 ($\Delta B = 0.25$ m and $b = 0.28$ m), 1.25 ($\Delta B = 0.35$ m and $b = 0.28$ m) and 4.38 ($\Delta B = 0.35$ m and $b = 0.08$ m). For each ratio, a large number of lengths were tested in order to find the transition between symmetric and asymmetric flows, and get information about the reattachment lengths.

The computational meshes were uniform Cartesian grids whose cell size was 0.010 m. In order to estimate the numerical uncertainty, simulations were also carried out with a cell size of 0.025 m for a small number of geometrical conditions.

Table 1 Dimensionless flow parameters.

Dimensionless parameter	Values investigated
$\frac{\Delta B}{b}$	0.52, 0.89, 1.25 and 4.38
$\frac{L}{\Delta B^{0.60} b^{0.40}}$	5.4–36.1
$\frac{h}{\Delta B}$	0.57 and 0.80
$\frac{U}{\sqrt{gh}}$	0.20
$\frac{4\rho U h}{\mu}$	220,000
$\frac{c_f \Delta B}{2h}$	0.002 and 0.003

In the present study, variable reconstruction at cell interfaces was performed linearly, leading to a second-order spatial accuracy. Since the model was applied to steady-state calculations, the time integration was performed by means of a three-step first order accurate Runge-Kutta algorithm, providing adequate dissipation in time. For stability reasons, the time step was constrained by the Courant-Friedrichs-Levy condition based on gravity waves.

The specific discharge was imposed as an inflow boundary condition ($q_0 = 0.056$ m^2/s) two meters upstream of the sudden expansion; its transverse value was set to zero. At the outlet (one meter downstream of the sudden contraction), a constant water surface elevation was imposed ($h = 0.20$ m). At the wall boundaries, the specific discharge normal to the wall was set to zero (impervious walls). The gradients in the direction parallel to the boundary were set at the same value as in the adjacent cell. The gradients in the direction normal to the boundary were evaluated differently for the velocity components normal and parallel to the boundary. In the former case, a finite difference was used between the value at the boundary and the value at the centre of the adjacent cell, whereas in the latter case the gradient was set to zero (Erpicum, 2006).

If the model does not include any spurious numerical artifact leading to asymmetry (such as the propagation of rounding errors), a problem with perfectly symmetric input data (equations, geometry, mesh, boundary and initial conditions) must lead to a symmetric solution; this was checked for the code Wolf 2D by Dewals et al. (2008). In order to give the flow the possibility of becoming asymmetric, one may introduce asymmetry into the problem through boundary and/or initial conditions. As Dewals et al. (2008) did for the inlet of the reservoir, the cross-sectional profile of the specific discharge at the inlet of the computational domain (namely two meters upstream of the inlet of the reservoir) was specified with a linear distribution:

$$q_{in,x}(y) = q_0\left(1 - \alpha_{BC}\frac{2y}{b}\right) \qquad q_{in,y}(y) = 0 \tag{3}$$

Here, $q_{in,x}(y)$ and $q_{in,y}(y)$ are the actual components specified as inflow boundary condition; q_0, the reference value (the total discharge divided by the width of the channel); α_{BC}, the amount of disturbance of the inlet boundary condition. It should be noted that y equals zero at the middle of the channel.

Asymmetry was also introduced through the initial flow field in the whole domain, as written in Eq. (4).

$$q_x(x,y) = 0$$
$$q_y(x,y) = -\alpha_{IC} q_0 \quad (4)$$

Here, $q_x(x,y)$ and $q_y(x,y)$ are the components of the initial specific discharge; α_{IC}, the amount of disturbance of the initial condition.

For all simulations, the initial water depth was set uniform with the same value as the outflow boundary condition, namely 0.20 m.

Because of the smooth bed and walls, the difference between downstream and upstream water depths was low (a few millimeters) for all the simulations. Therefore, 0.20 m and 0.28 m/s can be respectively used as representative water depth and depth-averaged velocity in the inlet channel.

3. SIMULATION PROTOCOL: BOUNDARY AND INITIAL CONDITIONS

Since one aim of the present paper is to investigate the transition between symmetric and asymmetric flows, a number of preliminary simulations were carried out for a geometrical condition located near the transition between S0 and A1 patterns in order to choose the protocol of simulation. The dimensions were chosen based on experimental results (Dufresne et al., 2010). The length was 2.40 m; the lateral expansion, 0.25 m; the width of the inlet and outlet channels, 0.30 m. This corresponds to a shape parameter of 8.9 (> 6.8). Results of these preliminary tests are given in Table 2.

When no asymmetry was introduced at all (neither in the boundary condition nor in the initial condition), the simulated flow was completely symmetric and exhibited two identical reattachment lengths (pattern S2). When asymmetry was introduced in the problem, even a small percentage of disturbance (0.1%) in the boundary or initial conditions was sufficient to obtain an asymmetric flow (pattern A1). Despite this result, a combination of a high disturbance in both boundary and initial conditions (10.0%) was chosen since this strategy led to a faster convergence.

This first protocol of simulation – named "Protocol 1" below – was therefore composed of two steps. Firstly, simulations were carried out with disturbances of 10.0% in both boundary and initial conditions. Secondly, in order to remove spurious artifacts due to high disturbance in the boundary condition (the reattachment length was 1.12 m for 0.1% and only 1.03 m for 10%, see Table 2), simulations were achieved with no disturbance in the boundary condition (α_{BC} = 0%). The reattachment length obtained using Protocol 1 is also 1.12 m (see Table 2).

A second simulation procedure, named "Protocol 2" below, was used in order to investigate the sensitivity of the numerical solution with respect to the initial condition, especially for reservoir geometries close to the transition between symmetric and asymmetric flow patterns. In this procedure, the asymmetric solution obtained for a reservoir of length L was used as the initial condition for simulating the flow in a reservoir of smaller length, say $L - \delta L$ (the last lines of cells are ignored, with all other cells retaining their previous values). Using a dichotomy procedure, if the flow obtained for the length $L - \delta L$ was found symmetric, the computation was restarted with a smaller value of δL. This was done until capturing the transition length with a step δL equal to the cell size (0.010 m). For Protocol 2, boundary conditions were always symmetric.

Before presenting the results using these two protocols and analyzing them, the next portion of the text is dedicated to the estimation of the numerical error.

Table 2 Influence of initial and boundary conditions for L = 2.40 m, ΔB = 0.25 m, b = 0.30 m.

α_{BC}	α_{IC}	Flow pattern	R_1 [m]
0.0%	0.0%	S2	1.94*
0.1%	0.0%	A1	1.12
1.0%	0.0%	A1	1.10
10.0%	0.0%	A1	1.03
0.0%	0.1%	A1	1.12
0.0%	1.0%	A1	1.12
0.0%	10.0%	A1	1.12
10.0%	10.0%	A1	1.03
Protocol 1		A1	1.12

* There were two symmetric reattachment lengths for this simulation.

Table 3 Numerical uncertainty for typical geometries.

	Test 1	Test 2	Test 3	Test 4
L [m]	7.00	7.00	6.50	2.40
ΔB [m]	0.35	0.25	0.25	0.25
b [m]	0.10	0.30	0.50	0.30
$\frac{\Delta B}{b}$	3.50	0.83	0.50	0.83
$\frac{L}{\Delta B^{0.60} b^{0.40}}$	33.0	26.0	19.7	8.9
Flow pattern	A2	A2	A2*	A1
R_1 [m] (coarse grid)	0.80	0.92	1.03*	0.98
R_1 [m] (fine grid)	0.94	1.03	1.15*	1.12
R_1 [m] (extrapolated)	0.97	1.05	1.17*	1.15
GCI (R_1)	8.8%	5.8%	5.1%*	6.2%
R_2 [m] (coarse grid)	4.14	2.92	2.74*	Ø
R_2 [m] (fine grid)	4.38	3.19	2.99*	Ø
R_2 [m] (extrapolated)	4.43	3.24	3.04*	Ø
GCI (R_2)	0.7%	1.5%	1.6%*	Ø

* The flow pattern obtained with the coarse grid using the protocol was symmetric (S2); therefore, the results presented here are those obtained at the end of the first step of Protocol 1.

4. NUMERICAL ERROR

Table 3 summarizes the simulated results obtained with a fine grid (cell size = 0.010 m) and a coarse grid (0.025 m). Four representative geometries were used: three "long" reservoirs (different lateral expansion ratios) for which the flow presented two asymmetric reattachment points, and one "short" reservoir (near the transition between symmetric and asymmetric flows) for which the flow exhibited one reattachment point. Since they should be multiples of 0.010 and 0.025 m, the dimensions of the four geometries are not exactly the experimental values (b = 0.10 m instead of 0.08 m, 0.30 instead of 0.28, and 0.50 instead of 0.48). Nevertheless, one can reasonably assume that the results can be transposed to the experimental dimensions. The number of cells corresponding to the meshes using for Test 1 (L = 7.00 m, ΔB = 0.35 m and b = 0.10 m) is approximately 60,000 for a cell size of 0.010 m and 10,000 for a cell size of 0.025 m.

The exact reattachment lengths were estimated using the Richardson extrapolation, as written in Eq. (5) (Roache, 1994) and given in Table 3.

$$R_{exact} \approx R_{fine} + \frac{R_{fine} - R_{coarse}}{r^p - 1} \tag{5}$$

Here, r is the grid refinement ratio (2.5); p, the actual order of accuracy (supposed to be equal to the formal order of accuracy, namely 2); R_{fine}, the reattachment length obtained for the fine grid; R_{coarse}, the reattachment length obtained for the coarse grid.

The grid convergence index (GCI), as proposed by Roache (1994), is written in Eq. (6).

$$GCI = \frac{3\left|\frac{R_{coarse} - R_{fine}}{R_{fine}}\right|}{r^p - 1} \tag{6}$$

The GCI was used to estimate the numerical error when using the fine grid (see Table 3): between 5% and 10% for the shorter reattachment length (R_1), lower than 2% for the longer one (R_2). The fine grid was used hereafter.

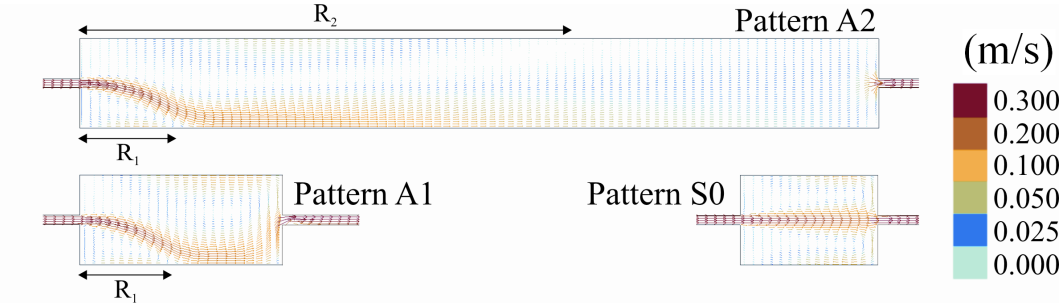

Fig. 3 Simulated flow patterns A2, A1 and S0 (b = 0.08 m; ΔB = 0.35 m; L = 7.00 m, 1.80 m and 1.20 m). R_1 and R_2 are respectively the shorter and the longer reattachment lengths.

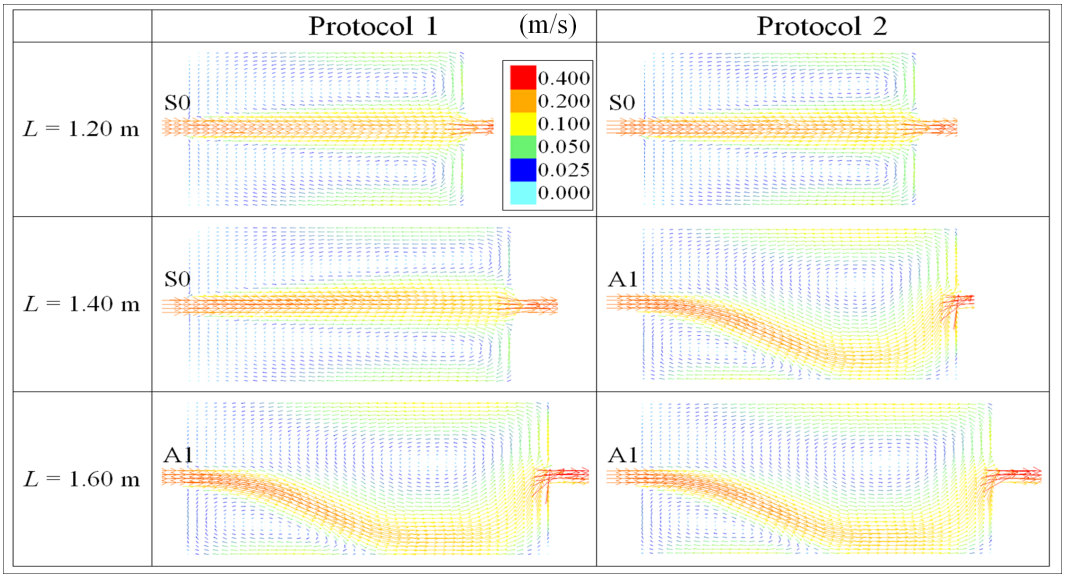

Fig. 4 Illustration of the sensitivity to the initial condition (b = 0.08 m; ΔB = 0.35 m).

5. RESULTS AND ANALYSIS

5.1 Description of flow fields

For lateral expansion ratios of 0.89, 1.25 and 4.38, small values of shape parameter correspond to the flow pattern S0 (Fig. 3): the jet entering the reservoir goes in a straight way to the exit and a circulation zone forms on each side of the jet. Increase of the shape parameter induces a sudden transition to asymmetric patterns (pattern A1). In these situations, the jet is deviated to one side at the entrance of the reservoir (always on the right for the simulations) and reattaches the wall at a distance R_1 from the inlet. For the longest reservoirs, the flow also reattaches on the opposite wall at a distance R_2 from the inlet (pattern A2). Illustrations of these simulated flow patterns are given in Fig. 3. Typical simulated flows are illustrated in Fig. 4.

The behavior is quite different for the smallest lateral expansion ratio (0.52). If patterns S0 are also encountered for small values of the shape parameter, increase of this dimensionless parameter induces a transition to the flow pattern S2: the flow is still symmetric but reattaches on both walls at the same distance, which was not experimentally observed. Further increasing the shape parameter leads to asymmetric flows with two different reattachment lengths (A2).

5.2 Assessment of effects due to simulation protocol

Table 4 gives the critical values of the shape parameter for the transition between symmetric and asymmetric flows. Since the length was not infinitely refined, some of these values are given as intervals. For example, the critical value for a lateral expansion ratio of 4.38 using Protocol 1 is 7.5–7.7; this means that the "last" asymmetric flow was obtained for a shape parameter of 7.7 (L = 1.50 m), that the "first" symmetric flow was obtained for a shape parameter of 7.5

(L = 1.45 m), and that no shape parameter between 7.5 and 7.7 was investigated. From this table, it can be seen that the simulated critical values of the shape parameter are overestimated compared to experiments (6.2–6.8), especially for small lateral expansion ratios. Whereas small values of lateral expansion ratio do not exhibit any significant sensitivity to the protocol of simulation, there is a large difference between the critical shape parameter obtained using Protocol 1 (7.5–7.7) and the one obtained using Protocol 2 (7.0) when the lateral expansion ratio is 4.38. Besides, the critical value obtained using Protocol 2 is relatively close to the upper limit of the experimental interval (approximately 6.8). This sensitivity to the initial condition is illustrated in Fig. 4: when the length of the reservoir is 1.40 m (shape parameter = 7.2), Protocol 1 leads to a symmetric flow whereas Protocol 2 leads to an asymmetric flow; for L = 1.20 m (6.2), both protocols lead to symmetric flows; for L = 1.40 m (8.2), they both lead to asymmetric flows.

Table 4 Critical values of the shape parameter (experimental value ≈ 6.2–6.8).

$\frac{\Delta B}{b}$	0.52	0.89	1.25	4.38
Protocol 1	9.2–9.7*	8.0–8.2	8.0–8.1	7.5–7.7
Protocol 2	-	8.0	8.0	7.0

* Transition between patterns S2 and A2.

5.3 Assessment of the influence of shape parameter on flow classification and reattachment lengths

Fig. 5 illustrates the comparison between the simulated and experimental reattachment lengths at different values of the lateral expansion ratio and the shape parameter. The experimental data points suggest that the shorter reattachment length (R_1) remains constant when the shape parameter is greater than a critical value (between 10 and 15, depending on the lateral expansion ratio); above this critical value, the shorter reattachment length is not influenced any more by the downstream wall of the reservoir (no longitudinal confinement).

For numerical simulations, decrease of the shape parameter near the transition from symmetric to asymmetric flows induces an increase of the reattachment length for lateral expansion ratios of 0.52, 0.89 and 1.25. For a lateral expansion ratio of 4.38, decreasing the shape parameter firstly induces a decrease of the reattachment length until it reaches a minimum level ($R_1/\Delta B \approx 2.2$); further decreasing the shape parameter causes a small increase of the dimensionless reattachment length until 2.3 (this corresponds to the difference between Protocol 1 and Protocol 2). The behavior was different for experiments: decreasing the shape parameter near the transition only caused an increase of the reattachment length for a lateral expansion ratio of 0.52; for 0.89, the reattachment length was almost constant; for 1.25 and 4.38, the reattachment length slightly decreased with the shape parameter (from approximately 3.4 to 3.1 for 1.25; from approximately 2.4 to 1.8 for 4.38).

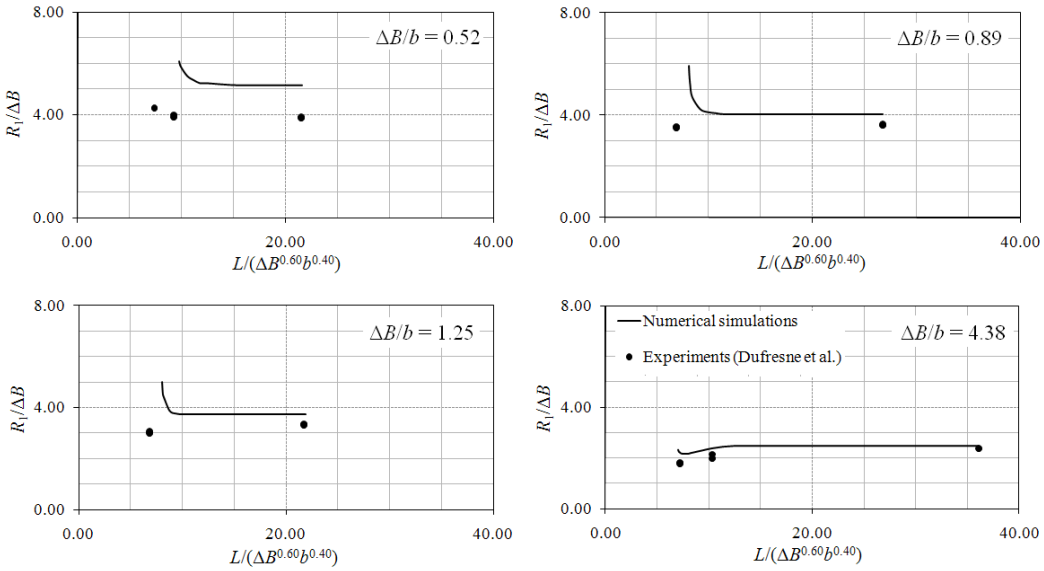

Fig. 5 Dimensionless reattachment length R_1 as a function of the shape parameter.

Comparison between simulated and experimental reattachment lengths highlights a relatively large discrepancy for small values of the lateral expansion ratio: around 30% for 0.52, around 10% for 0.89 and 1.25 (for large values of shape parameter). For 4.38, the error between simulations and experiments is small (around 5% for a shape parameter of 36.1); given the numerical uncertainty (see Table 3, Test 1), it can be concluded that there is a good agreement between the numerical and experimental shorter reattachment lengths for large values of lateral expansion ratio and shape parameter. Near the transition, even for a lateral expansion ratio of 4.38, the difference between simulations and experiments is relatively significant (around 20%).

The discrepancy between experimental and numerical reattachment length can be explained as follows. First, the experimental results revealed a small unsteadiness of the reattachment length around its median position (Dufresne et al., 2010), which cannot be reproduced by the model. Second, the effect of flow curvature on bed friction due to enhanced vertical mixing induced by horizontal strain rates is not taken into account by the model, which may considerably underestimate the bed friction in some cases (Stanby, 2003 & 2006).

Only three measurements were carried out for the longer reattachment length (Dufresne et al., 2010): $R_2/\Delta B = 18.3$ (simulated result: 13.2) when $\Delta B/b = 1.25$ and $L/(\Delta B^{0.60} b^{0.40}) = 21.9$; $R_2/\Delta B = 10.0$ (simulated result: 10.5) when $\Delta B/b = 0.52$ and $L/(\Delta B^{0.60} b^{0.40}) = 21.6$; $R_2/\Delta B = 9.6$ (the simulated result corresponds to a flow pattern S2) when $\Delta B/b = 1.25$ and $L/(\Delta B^{0.60} b^{0.40}) = 9.2$. This dataset is not sufficient to draw any conclusion on the longer reattachment length.

6. PREDICTION

Since there was a good agreement between numerical simulations and experiments for the transition between symmetric and asymmetric flows for large values of $\Delta B/b$ and the reattachment length R_1 for large values of $\Delta B/b$ and $L/\Delta B^{0.60} b^{0.40}$, the model was used as a prediction tool to get information about larger values of lateral expansion ratio that can be encountered for real-life reservoirs. This study was not conducted experimentally because of the limited dimensions of the experimental setup (Dufresne et al., 2010).

Three values of $\Delta B/b$ were investigated to extend the experimental data: 5.00, 7.50 and 10.00 (with $b = 0.08$ m). For each ratio, simulations were carried out in order to find the transition between symmetric and asymmetric flows and also to get information about the shorter reattachment length when it is not sensitive any more to the shape parameter.

As given in Table 5, the comparison of the critical shape parameters using Protocol 1 and Protocol 2 highlights a significant sensitivity to the initial condition. Whereas the critical values obtained with Protocol 1 are scattered, the critical values obtained with Protocol 2 are relatively close to 7.0 (7.0 for $\Delta B/b = 5.00$, 7.1 for 7.50 and 7.3 for 10.00). Despite the slight increase of the critical value with increase of the lateral expansion ratio, additional simulations for larger $\Delta B/b$ would be required to really argue in favor of modifying the shape criterion. In other words, this means that the shape parameter – which has been defined only based on experiments for values of $\Delta B/b$ between 0.52 and 4.38 – is also relevant for $\Delta B/b$ up to 10.00.

Table 5 Prediction of the critical values of the shape parameter (experimental value ≈ 6.2–6.8).

$\frac{\Delta B}{b}$	5.00	7.50	10.00
Protocol 1	7.6–7.9	8.8–9.0	8.2–8.3
Protocol 2	7.0	7.1	7.3

Fig. 6 shows the shorter reattachment length from both laboratory experiments and numerical simulations. Simulations were carried out for $L/\Delta B^{0.60} b^{0.40}$ of 38.1 ($\Delta B/b = 5.00$), 44.8 (7.50) and 50.2 (10.00); these values are significantly higher than the critical shape parameter highlighted by Fig. 5 (in the interval 10 – 15). Given the numerical uncertainty of the shorter reattachment length, the agreement between the simulated values and the regression only based on experimental measurements is very good for large values of lateral expansion ratio (< 5%):

$$R_1 \approx 3.43 \Delta B^{0.75} b^{0.25} \quad (7)$$

This equation is only valid when $\Delta B/b$ is greater than 0.52 and lower than 10.00. Fig. 6 also suggests that a limiting plateau value of $R_1/\Delta B \approx 2$ can be assumed from the data trend for $\Delta B/b$.

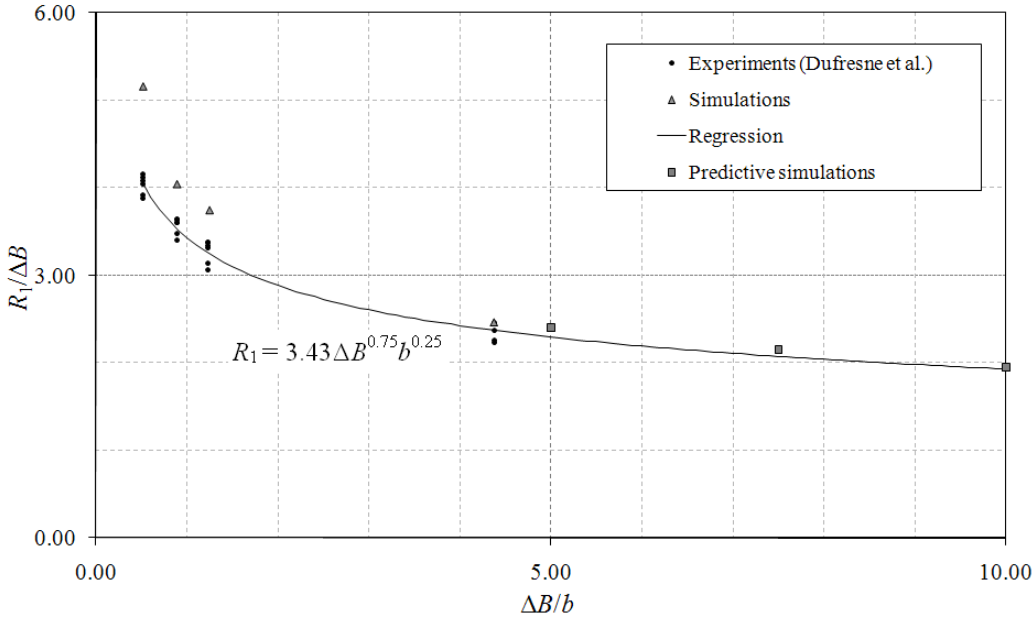

Fig. 6 Dimensionless reattachment length as a function of the lateral expansion ratio.

7. CONCLUSIONS

In the present study, the capability of a two-dimensional shallow-water numerical model to simulate the symmetric and asymmetric flows that can take place in rectangular shallow reservoirs with different lateral expansion ratios and dimensionless lengths was investigated. The use of the Colebrook friction model and the k-ε turbulent model freed us of any calibration procedure.

Two protocols of simulation were used. Protocol 1 was composed of two steps: simulation was first carried out with disturbances of 10.0% in both boundary and initial conditions; it was then achieved with no disturbance in the boundary condition in order to remove spurious artifacts. Protocol 2 was defined as follows: the asymmetric solution obtained for a reservoir of length L was used as the initial condition for simulating the flow in a reservoir of smaller length, say $L - \delta L$. For Protocol 2, boundary conditions were always symmetric.

For a lateral expansion ratio of 4.38, the use of Protocol 1 and Protocol 2 highlighted a high sensitivity of the critical shape parameter ($L/\Delta B^{0.60} b^{0.40}$) to the initial condition. When using Protocol 2, the transition between symmetric and asymmetric flows occurred around a shape parameter 7.0, which was relatively close to the upper limit of the experimental interval (approximately 6.8). Therefore, Protocol 2 should be preferred to Protocol 1. It has also been shown that the model accurately reproduces the shorter reattachment length R_1 for $\Delta B/b = 4.38$. For smaller values of lateral expansion ratio (0.52, 0.89 and 1.25), the agreement between experimental and numerical critical shape parameters and reattachment lengths was not so good.

Based on these results, the model was used for larger lateral expansion ratios in order to numerically extend the experimental data. This predictive work showed that the shape parameter, whose expression was only based on experiments undertaken for $\Delta B/b$ between 0.52 and 4.38, was also relevant up to 10.00. Moreover, the predicted values of the shorter reattachment length for large shape parameters were also consistent with the regression only based on experimental results.

A great attention must be paid to the simulation protocol since symmetric and asymmetric flow patterns may be responsible for completely different deposition patterns; this will be numerically investigated in the near future.

ACKNOWLEDGEMENTS

The authors would like to acknowledge the University of Liège for the allocation of a postdoctoral fellowship to the first author.

REFERENCES

1. Abbott DE, Kline SJ (1962). Experimental investigation of subsonic turbulent flow over single and double backward facing steps. *Journal of Basic Engineering* 84:317–325.
2. Babarutsi S, Chu VH (1991). Dye-concentration distribution in shallow recirculating flows. *Journal of Hydraulic Engineering* 117:643–659.
3. Babarutsi S, Chu VH (1998). Modeling transverse mixing layer in shallow open-channel flows. *Journal of Hydraulic Engineering* 124(7):718–727.
4. Babarutsi S, Ganoulis J, Chu VH (1989). Experimental investigation of shallow recirculating flows. *Journal of Hydraulic Engineering* 115:906–924.
5. Battaglia F, Papadopoulos G (2006). Bifurcation characteristics of flows in rectangular sudden expansion channels. *Journal of Fluids Engineering* 128:671–679.
6. Casarsa L, Giannattasio P (2008). Three-dimensional features of the turbulent flow through a planar sudden expansion. *Physics of Fluids* 20:5103:1–15.
7. Chu VH, Liu F, Altai W (2004). Friction and confinement effects on a shallow recirculating flow. *Journal of Environmental Engineering and Science* 3:463–475.
8. De Zilwa SRN, Khezzar L, Whitelaw JH (2000). Flows through plane sudden-expansions. *International Journal for Numerical Methods in Fluids* 32:313–329.
9. Dewals BJ (2006). *Une approche unifiée pour la modélisation d'écoulements à surface libre, de leur effet corrosif sur une structure et de leurs interactions avec divers constituants*. PhD thesis, Université de Liège (in French).
10. Dewals BJ, Kantoush SA, Erpicum S, Pirotton M, Schleiss AJ (2008). Experimental and numerical analysis of flow instabilities in rectangular shallow basins. *Environmental Fluid Mechanics* 8:31–54.
11. Dufresne M (2008). *La modélisation 3D du transport solide dans les bassins en assainissement : du pilote expérimental à l'ouvrage réel* [*Three-dimensional modelling of sediment transport in sewer detention tanks: physical model and real-life application*]. PhD thesis, Université de Strasbourg (in French).
12. Dufresne M, Dewals BJ, Erpicum S, Archambeau P, Pirotton M (2010). Classification of flow patterns in rectangular shallow reservoirs. *Journal of Hydraulic Research* 48:197–204.
13. Erpicum S (2006). *Optimisation objective de paramètres en écoulements à surface libre sur maillage multibloc*. PhD thesis, Université de Liège (in French).
14. Erpicum S, Dewals BJ, Archambeau P, Pirotton M (2010). Dam-break flow computation based on an efficient flux-vector splitting. *Journal of Computational and Applied Mathematics* 234(7):2143-2151.
15. Erpicum S, Meile T, Dewals BJ, Pirotton M, Schleiss AJ (2009). 2D numerical flow modeling in a macro-rough channel. *International Journal for Numerical Methods in Fluid* 61(11):1227-1246.
16. Garde RJ, Ranga Raju KG, Sujudi AWR (1990). Design of settling basins. *Journal of Hydraulic Research* 28(1):81–91.
17. Henderson FM (1966). *Open channel flow*. Prentice Hall: New York.
18. Idel'cik IE (1969). *Mémento des pertes de charge*, Eyrolles (translated to French by Meury M).
19. Jothiprakash V, Garg V (2008). Re-look to conventional techniques for trapping efficiency estimation of a reservoir. *International Journal of Sediment Research* 23(1):76–84.
20. Kantoush SA (2008). *Experimental study on the influence of the geometry of shallow reservoirs on flow patterns and sedimentation by suspended sediments*. PhD thesis, Ecole Polytechnique Fédérale de Lausanne.
21. Kantoush SA, De Cesare G, Boillat JL, Schleiss AJ (2008a). Flow field investigation in a rectangular shallow reservoir using UVP, LSPIV and numerical modelling. *Flow Measurement and Instrumentation* 19:139–144.
22. Kantoush SA, Bollaert E, Schleiss AJ (2008b). Experimental and numerical modelling of sedimentation in a rectangular shallow basin. *International Journal of Sediment Research* 23:212–232.
23. Kowalski R, Reuber J, Köngeter J (1999). Investigations into and optimisation of the performance of sewage detention tanks during storm rainfall events. *Water Science and Technology* 39(2):43–52.
24. Langhaar HL (1951). *Dimensional analysis and theory of models*. John Wiley & Sons: New York.
25. Luyckx G, Vaes G, Berlamont J (1999). Experimental investigation on the efficiency

of a high side weir overflow. *Water Science and Technology* 39(2):61–68.
26. Mizushima J, Shiotani Y (2001). Transitions and instabilities of flow in a symmetric channel with a suddenly expanded and contracted part. *Journal of Fluid Mechanics* 434:355–369.
27. Mullin T, Shipton S, Tavener SJ (2003). Flow in a symmetric channel with an expanded section. *Fluid Dynamics Research* 33:433–452.
28. Oca J, Masaló I, Reig L (2004). Comparative analysis of flow patterns in aquaculture rectangular tanks with different water inlet characteristics. *Aquacultural Engineering* 31:221–236.
29. Ranga Raju KG, Kothyari UC, Srivastav S, Saxena M (1999). Sediment removal efficiency of settling basins. *Journal of Irrigation and Drainage Engineering* 125(5):308–314.
30. Revuelta A (2005). On the two-dimensional flow in a sudden expansion with large expansion ratios. *Physics of Fluids* 17:1–4.
31. Roache PJ (1994). Perspective: a method for uniform reporting of grid refinement studies. *Journal of Fluids Engineering* 116:405– 413.
32. Roger S, Dewals BJ, Erpicum S, Schwanenberg D, Schüttrumpf H, Köngeter J, Pirotton M (2009). Experimental und numerical investigations of dike-break induced flows. *Journal of Hydraulic Research* 47(3):349–359.
33. Stanby PK (2003). A mixing length model for shallow turbulent wakes. *Journal of Fluid Mechanics* 495:369–384.
34. Stanby PK (2006). Limitations of depth-averaged modelling of shallow wakes. *Journal of Hydraulic Engineering* 132:737–740.
35. Stovin VR, Saul AJ (1994). Sedimentation in storage tank structures. *Water Science and Technology* 29:363–372.
36. Takaoka M, Sano T, Yamamoto H, Mizushima J (2009). Convective instability of flow in a symmetric channel with spatially periodic structures. *Physics of Fluids* 21:1–10.
37. Todeschini S, Ciaponi C, Papiri S (2010). Laboratory experiments and numerical modelling of the scouring effects of flushing waves on sediment beds. *Engineering Applications of Computational Fluid Mechanics* 4(3):365–373.
38. Uijttewaal WSJ, Lehmann D, Van Mazijk A (2001). Exchange processes between a river and its groyne fields: model experiments. *Journal of Hydraulic Engineering* 127:928–936.
39. Wahba EM (2007). Iterative solvers and inflow boundary conditions for plane sudden expansion flows. *Applied Mathematical Modelling* 31:2553–2563.
40. Yang YT, Hou CF (1999). Numerical calculation of turbulent flow in symmetric two-dimensional diffusers. *Acta Mechanica* 137:43–54.
41. Yeo HK, Kang JG, Kim SJ (2005). An experimental study on tip velocity and downstream recirculation zone of single groynes of permeability change. *KSCE Journal of Civil Engineering* 9:29–38.